

Magnetization of the spin-1/2 Heisenberg antiferromagnet on the triangular lattice

Qian Li,¹ Hong Li,² Jize Zhao,^{1,*} Hong-Gang Luo,^{1,3} and Z. Y. Xie^{2,†}

¹*School of Physical Science and Technology & Key Laboratory for Magnetism and Magnetic Materials of the MoE, Lanzhou University, Lanzhou 730000, China*

²*Department of Physics, Renmin University of China, Beijing 100872, China*

³*Beijing Computational Science Research Center, Beijing 100084, China*

After decades of debate, now there is a rough consensus that at zero temperature the spin-1/2 Heisenberg antiferromagnet on the triangular lattice is three-sublattice 120° magnetically ordered, in contrast to a quantum spin liquid as originally proposed. However, there remains considerable discrepancy in the magnetization reported among various methods. To resolve this issue, in this work we revisit this model by the tensor-network state algorithm. The ground-state energy per bond E_b and magnetization per spin M_0 in the thermodynamic limit are obtained with high precision. The former is estimated to be $E_b = -0.18334(10)$. This value agrees well with that from the series expansion. The three-sublattice magnetic order is firmly confirmed and the magnetization is determined as $M_0 = 0.161(5)$. It is about 32% of its classical value and slightly below the lower bound from the series expansion. In comparison with the best estimated value by Monte Carlo and density-matrix renormalization group, our result is about 20% smaller. This magnetic order is consistent with further analysis of the three-body correlation. Our work thus provides new benchmark results for this prototypical model.

I. INTRODUCTION

One challenging task in modern condensed matter physics is to search for exotic states of matter both experimentally and theoretically. In this long journey, systems with geometric frustration have emerged as a flourishing research area. In usual magnets, spins freeze into some periodic patterns upon cooling, associated with a phase transition from a paramagnetic phase to an ordered phase. The transition temperature, in comparison with the Curie-Weiss temperature, may be drastically suppressed by geometric frustration. Actually, in 1973, P. W. Anderson already proposed that some frustrated magnets may remain disordered even at zero temperature, which is now known as the quantum spin liquid [1–5]. Ever since then, a large amount of interest has been attracted to search for such exotic states [6, 7]. Particularly, in Anderson’s original paper [1], the spin-1/2 antiferromagnetic Heisenberg model on the triangular lattice (TAHM) was conjectured to be such a candidate. Moreover, Anderson proposed that its ground state may be a resonating valence-bond state (RVB) rather than a state with three-sublattice 120° magnetic order (TMO) in its classical counterpart.

In the past decades, to clarify the nature of its ground state, TAHM has been extensively studied by a variety of analytical and numerical methods [8–29]. For example, Huse and Elser examined this model by variational Monte Carlo [8]. They chose a trial wavefunction with three-spin terms. By comparing its ground-state energy with that of RVB-type wavefunctions, they found that the former is energetically favored, and its magnetization is finite,

about 68% of its classical value. On small clusters, exact diagonalization (ED) calculations were performed by several groups but their conclusions are conflicting [11–14]. The Green’s function Monte Carlo (GFMC) [15] and density-matrix renormalization group (DMRG) [16] calculations, which were on moderate clusters, concluded the existence of an ordered ground state with a consistent magnetization $M_0 \approx 0.205$. As far as we know, so far the smallest but finite magnetization reported is $M_0 = 0.1625(30)$, obtained by GFMC with fixed node approximation [17]. Now it is mostly believed that the ground state of the TAHM is a TMO state with strongly suppressed magnetization.

However, whereas such progress has been made, the debate has never ceased completely so far. For example, recent numerical analyses based on bold diagrammatic Monte Carlo [18] and ED [14] supported the absence of magnetic order. Moreover, even in those works supporting the existence of TMO, the discrepancy of the magnetization is quite large, with its value ranging from 0.1625(30) to 0.36 [17, 19]. And finally, from the experimental perspective, various compounds with triangular geometry have been synthesized and fingerprints of quantum spin liquids were reported [30, 31], but their nature remains controversial. As a prototypical model with geometric frustration, precise understanding of the TAHM is important and necessary. In particular, an accurate estimate of the magnetization may help us to understand related experiments and serve as a benchmark for newly developed numerical algorithms. It is fair to say that the present knowledge remains unsatisfactory and thus calls for further studies on this model.

For this purpose, we revisit this model by tensor-network state (TNS) method [32–34] which is under rapid development and has drawn great attention due to its successful applications in strongly-correlated condensed matter physics [35–37], statistical physics [38–40], quan-

*zhaojz@lzu.edu.cn

†qingtaoxie@ruc.edu.cn

tum field theory [41–43], and machine learning [44, 45], etc. To be specific, the TAHM is described by the Hamiltonian

$$\mathcal{H} = J \sum_{\langle ij \rangle} \hat{\mathbf{S}}_i \cdot \hat{\mathbf{S}}_j, \quad (1)$$

where $J > 0$ is the antiferromagnetic coupling. Hereafter we set $J = 1$ as the energy unit. $\hat{\mathbf{S}}_i$ is the spin operator at site i . $\langle \dots \rangle$ means a summation over the nearest-neighbor pairs. We use the projected entangled simplex state (PESS) ansatz [46] to represent the ground-state wavefunction, and employ the corner transfer-matrix renormalization group (CTMRG) method [36, 47, 48] to estimate the physical quantities, such as E_b , M_0 , and many-body correlation [49].

The rest of the paper is organized as follows. In Sec. II, we introduce some details of the algorithm employed in our work. The numerical results for E_b , M_0 and many-body correlation are present in Sec. III. In Sec. IV, we summarize our work.

II. METHODS

Frustration in TAHM makes it difficult to be investigated with traditional numerical methods such as Monte Carlo, which suffers from the infamous sign problem and strong finite-size effect. Generally, the TNS method is free of the sign problem and can study this model in the thermodynamic limit directly by assuming a translationally invariant wavefunction. Therefore, it is drawing increasing attention nowadays.

In the TNS family, PESS is a wavefunction ansatz [46] generalized from the popular projected entangled pair state [34], and is believed to be suitable for frustrated systems. In this work, the PESS ansatz is defined as

$$|\Psi\rangle = \sum_{\{\sigma\}} \text{Tr}(\dots S_{i_{\mu\nu}j_{\mu\nu}k_{\mu\nu}}^{(\mu\nu)} A_{i_{\lambda\omega}j_{\lambda\omega}k_{\lambda\omega}}^{(\lambda\omega)}[\sigma_{\lambda\omega}]\dots) |\dots \sigma_{\lambda\omega} \dots\rangle \quad (2)$$

which is illustrated in Fig. 1. Here (μ, ν) denotes the location of the upward triangles, and (λ, ω) denotes the location of the lattice sites. A rank-3 simplex tensor S is defined at the center of each upward triangle, and a rank-4 projection tensor A is defined at each lattice site. $\{i, j, k\}$ and $\{\sigma\}$ are the virtual indices and physical basis associated with the tensors, respectively. The two virtual indices associated with the same bond take the same values. Tr is over all the repeated virtual indices and \sum is over all the basis configurations.

To employ the translational invariance, we use a 3×3 periodicity, which means that

$$S^{(\mu, \nu)} = S^{(\mu+3m, \nu+3n)}, \quad A^{(\lambda, \omega)} = A^{(\lambda+3m, \omega+3n)} \quad (3)$$

where m, n are integers. In other word, we totally have 9 different S and 9 different A in the ansatz (2). The corresponding unit cell is illustrated by a dashed rhombus in Fig. 1.

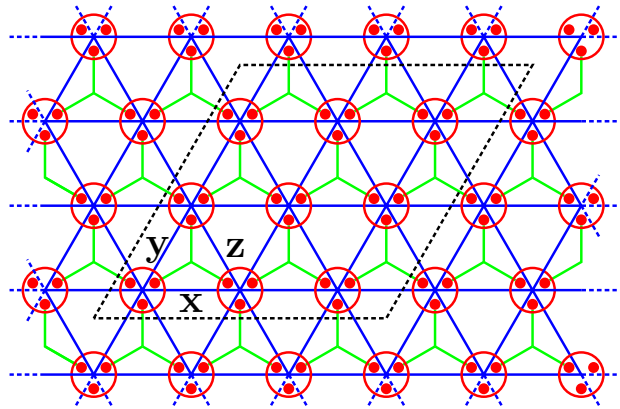


FIG. 1: Schematic diagram of the PESS wavefunction ansatz on the infinite triangular lattice. The blue lines are the bonds of the lattice, which are marked by x, y and z , respectively. The green lines represent virtual bonds of the wavefunction. The tensors sitting at the center of the triangles are the simplex tensors S , and the tensors covered by red circle are the projection tensors A . The rhombus with dashed lines marks a 3×3 unit cell of the trial wave function. The physical indices are perpendicular to the plane and not shown here.

It is known that the bond dimension, D , which is the maximal value of the virtual indices, controls the number of independent parameters and thus the numerical accuracy. In this work, D is up to 13. The ground-state wavefunction is optimized by simple update algorithm [50, 51]. Though the full update strategy [52] might be more accurate, it is much more costly. By comparing their results for a moderate D , e.g., $D = 6$, we found the difference was negligible. Therefore, in viewing of the computational cost, we use the more efficient simple update scheme in this work. In order to avoid bias and reduce the Trotter error, we started from a wavefunction randomly generated in complex field, and gradually reduced the Trotter step τ from a large value, say 0.2. The final τ is smaller than 10^{-3} , which turns out to be sufficiently small to estimate the magnetization of TAHM.

Physical observables are calculated via the CTMRG method, which was developed for an arbitrary unit cell on the square lattice [36]. In Fig. 1, we show the PESS ansatz defined on honeycomb skeleton. Firstly, we formally deform the skeleton to a square by simply combining S with A together to form a single tensor T , e.g.,

$$T_{k_1 k_2 i_1 i_2}^{(\mu\nu)}[\sigma] = \sum_j S_{i_1 j k_1}^{(\mu\nu)} A_{i_2 j k_2}^{(\mu, \nu+1)}[\sigma] \quad (4)$$

This is done in all the upward triangles coherently, as illustrated in Fig. 2(a). Hence, the reduced network $\langle \Psi | \Psi \rangle$, which appears in expectation value calculation, see Eq. (5) and (6), can be represented as a two-dimensional tensor network with a 3×3 periodicity, as illustrated in Fig. 2(b), and then the standard CTMRG method can be applied directly to contract the network. Finally the local physical observables can be

calculated efficiently from the local environment tensors $\{L, R, U, D, C\}$. Similarly, the bond dimension χ of the environment tensors is a tunable parameter which controls the accuracy in CTMRG. In our calculation, the maximal χ is no less than D^2 to ensure a reliable result [53].

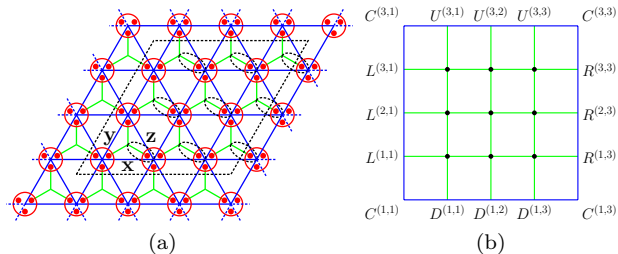


FIG. 2: (a) Converting the tensor network skeleton from the honeycomb lattice to a square lattice by one-step contraction, e.g., in the direction of the bonds surrounded by dashed ellipses. (b) The 3×3 unit cell obtained after deformation in the reduced network $\langle \Psi | \Psi \rangle$. Here the environment tensors of the unit cell are shown explicitly, e.g., $L^{(3,1)}$ are the edge tensor associated with the left of $T^{(3,1)}$.

III. RESULTS

A. Ground-State Energy

The ground-state energy usually serves as a key criterion for trial wavefunctions, particularly in the variational Monte Carlo simulations. This is exactly how Huse and Elser excluded the quantum spin liquid ground state in TAHM [8]. From this aspect, an accurate estimate of the ground-state energy is important. Therefore, firstly we need to check whether our numerical results are reliable, by comparing the ground-state energy with that in previous works.

The ground-state energy for a given bond $\langle ij \rangle$ is given by

$$E_{\langle ij \rangle} = \frac{\langle \Psi | \hat{\mathbf{S}}_i \cdot \hat{\mathbf{S}}_j | \Psi \rangle}{\langle \Psi | \Psi \rangle} \quad (5)$$

where $|\Psi\rangle$ is the PESS representation of the ground-state wavefunction, see Eq. (2). Since our system is translationally invariant, the bond energy E_b can be estimated by averaging $E_{\langle ij \rangle}$ over all bonds in one unit cell.

As stated in the previous section, the accuracy of the wavefunction is controlled by D , and that of the expectation is controlled by χ . Therefore, to obtain accurate results for a given D , the expectation values are calculated with a series of χ in which the largest one is no less than D^2 , and then extrapolated as $\chi \rightarrow \infty$.

For the smallest $D = 4$ in our simulations, the ground-state energy is $-0.18226(9)$, which is already smaller than that obtained by GFMC [15], $-0.18193(3)$. To provide an

intuitive impression, in Fig. 3, we plot the energy E_b as a function of $1/\chi$ for $D = 10, 11, 12$ and 13 . It seems that E_b depends very weakly on D when χ becomes large, and all the data points are well below those from GFMC.

As χ increases, E_b roughly decreases monotonically, but they oscillate in a small interval as a function of D . For the data points with largest χ in Fig. 3, E_b is between -0.18328 and -0.18336 . With the available χ , this non-monotonic behavior with regard to D makes it difficult to extrapolate our data and hinder us to obtain more accurate results. As a compromise, we firstly extrapolate the data for $D = 10, 11, 12$ and 13 to the infinite χ limit, respectively, and then average them. Our final result is $E_b = -0.18334(10)$, which agrees well with that obtained by the series expansion (SE) [21] and the coupled cluster method [28].

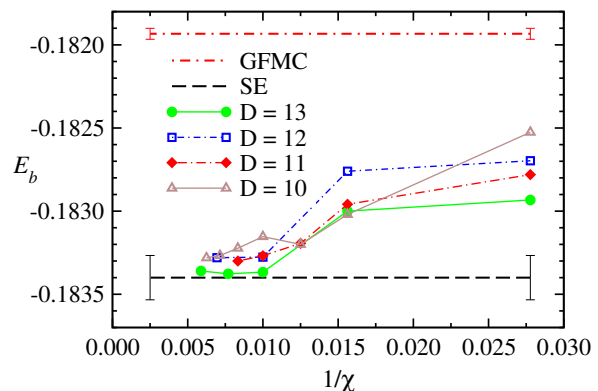


FIG. 3: The ground-state energy for $D = 10, 11, 12$ and 13 is plotted as a function of χ . The numerical error is on the fifth digit and they are not shown for a clear vision. The data obtained by GFMC [15] and SE [21] are also shown for comparison. Our data are obviously below that from GFMC but agrees well with that by SE (within the error bar).

In Tab. I, we summarize some recent works for comparison. These data indicate that our PESS wavefunction represents a good approximation of the ground state of TAHM.

B. Magnetization

The main debate about this model is whether the ground state is a TMO state or a quantum spin liquid. From Tab. I, we can see that, even in those works advocating TMO, the magnetization M_0 differs significantly. For example, if the error bar is taken into account, the low bound given by SE [26] is smaller than half of that given in Ref. [19]. This motivates us to calculate the magnetization in this work. Given the ground state $|\Psi\rangle$, three components of the magnetization vector \vec{M}_i at the

Method	E_b	M_0	Year
this work	-0.18334(10)	0.161(5)	2020
SB+1/N [29]	—	0.224	2018
CC [28]	-0.1838	0.21535	2016
SB [26]	—	0.2739	2015
SWT [26]	—	0.2386	2015
SE [26]	—	0.198(34)	2015
CC [27]	-0.18403(7)	0.198(5)	2015
CC [24]	-0.1843	0.1865	2014
VMC [25]	-0.18163(7)	0.2715(30)	2014
SWT [23]	-0.18228	0.24974	2009
VMC [22]	-0.18233(3)	0.265	2009
DMRG [16]	—	0.205(15)	2007
FN [17]	-0.17996(1)	0.1625(30)	2006
FNE [17]	-0.18062(2)	0.1765(35)	2006
SE [21]	-0.18340(13)	0.19(2)	2006
VMC [19]	-0.1773(3)	0.36	2006
ED [13]	-0.1842	0.193	2004
DMRG [20]	-0.1814	—	2001
GFMC [15]	-0.18193(3)	0.205(10)	1999

TABLE I: E_b and M_0 obtained by various methods are shown for comparison. SB, CC, SWT, VMC, FN, and FNE denote Schwinger boson mean field theory, coupled cluster, spin-wave theory, variational Monte Carlo, fixed node, and fixed node with effective Hamiltonian, respectively.

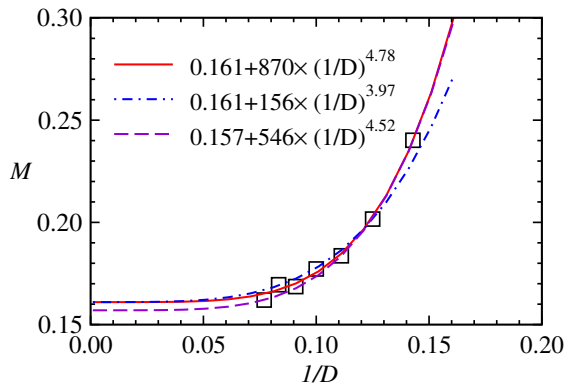


FIG. 4: M , marked as \square , is plotted as a function of $1/D$. All the data points have already been extrapolated to the infinite- χ limit. The lines are different numerical fittings: solid line is obtained from all D , while dot-dashed line and dashed line are obtained from even and odd D only, respectively.

site i are given by

$$M_i^\alpha = \frac{\langle \Psi | \hat{S}_i^\alpha | \Psi \rangle}{\langle \Psi | \Psi \rangle}, \quad \alpha = x, y, z \quad (6)$$

from which the magnetization at site i reads

$$M_i = \sqrt{(M_i^x)^2 + (M_i^y)^2 + (M_i^z)^2},$$

and the relative angles between neighbouring spins are immediately available. In the calculation, we found that the magnetization is almost independent of the sites. For simplicity, hereafter we show only the overall magnetization M , which is obtained by averaging over all the M_i within one unit cell. Similar to the calculation of E_b , for a given D , we extrapolate M as a function of $1/\chi$ to the infinite χ limit.

The results for D from 7 to 13 are illustrated in Fig. 4. We notice that for $D = 9$, our result is already smaller than most of recent results, see Tab. I. Clearly, it shows that M decreases roughly as a monotonic function of $1/D$. To get a more accurate estimate, we try to fit them with two typical formulae. One is an power-law formula, i.e., $M = M_0 + a \times (1/D)^b$, yielding $M_0 = 0.161$. The other is an exponential formula, i.e., $M = M_0 + a \times \exp(-bD)$, with $M_0 = 0.164$ for the best fit.

With a careful inspection of Fig. 4, we notice that there is a tiny even-odd oscillation in the magnetization as a function of D , which suggests us fit the magnetization for even and odd D separately. Using the power-law formula, we obtain $M_0 = 0.161$ and $M_0 = 0.157$ for even and odd D , respectively. Defining the error bar as the standard deviation among the four different M_0 obtained above, we conclude that $M_0 = 0.161(5)$, which is very close to the lower bound obtained by SE [21, 26]. One may notice that this value is also very close to that in Ref. [17], but their ground-state energy is obviously not optimal. More details can be found in Tab. I.

We would like to emphasize that the magnetization we obtained is slightly smaller than $1/3$ of its classical value. In particular, it is smaller than all that obtained in previous works. On one hand, such a small magnetization requires a careful finite-size analysis to obtain a quantitatively reliable estimation in numerical calculations such as the ED, DMRG, and Monte Carlo. On the other hand, generally, TNS method usually tends to overestimate the magnetization in frustrated systems when D is finite [37]. This suggests that probably our smallest result for finite D is the upper bound of the magnetization. Therefore, it is quite likely that M_0 has been overestimated in previous works.

In Tab. II, we present the data of the angles between all the nearest neighbors in the unit cell, for two sets of parameters, i.e., $D = 4$ with $\chi = 32$ and $D = 13$ with $\chi = 170$. It shows that: (I) the 120° angles between nearest neighbors are almost perfect, in the sense that the largest error bar is as small as 0.021° with D up to 13, (II) in contrast to the magnetization, the angles are almost independent of D and χ , as long as they are not too small. Therefore, we can safely conclude the existence of the TMO.

(μ, ν)	$D = 4, \chi = 32$			$D = 13, \chi = 170$		
	x	y	z	x	y	z
(1, 1)	120.004	120.000	119.996	120.010	119.988	120.002
(1, 2)	119.999	120.000	120.001	119.985	119.994	120.021
(1, 3)	119.997	120.000	120.003	120.005	119.993	120.002
(2, 1)	120.004	120.000	119.996	120.005	120.012	119.983
(2, 2)	119.999	120.000	120.001	119.992	120.013	119.994
(2, 3)	119.997	120.000	120.003	120.004	120.013	119.983
(3, 1)	120.004	120.000	119.006	120.003	120.001	119.996
(3, 2)	119.999	120.000	120.001	119.993	120.993	119.986
(3, 3)	119.997	120.000	120.003	120.004	119.994	120.998

TABLE II: Angles (in unit of degree) of the magnetization vectors between nearest neighbors are shown. Location of the upward triangles in the unit cell is listed explicitly. x, y and z are the three directions in the triangle lattice, as marked in Fig. 1. They indicate the corresponding bonds of the triangle here.

C. Larger Unit Cell

The result of TNS simulation might also depend on the size of the unit cell, thus we need to check whether the unit cell we used in the wavefunction ansatz is sufficiently large. For this purpose, we compare our results from the 3×3 unit cell with those from the 6×6 unit cell. In Fig. 5, we plot E_b and M as a function of χ for $D = 10$ and 6. The data is in excellent agreement for the two different unit cells, and the differences at all data points are negligible compared to the error bar. This suggests that the 3×3 unit cell in our work is already large enough for TAHM.

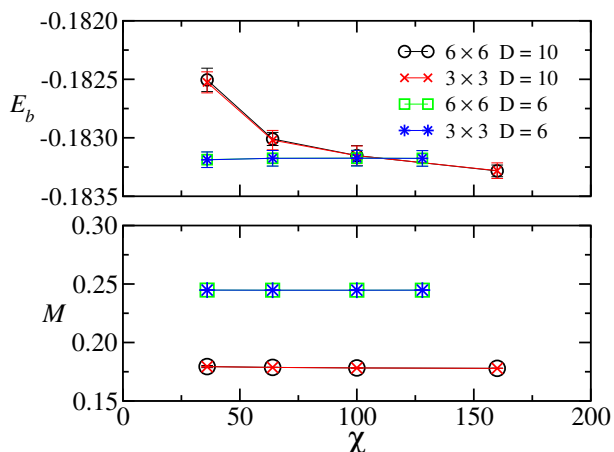


FIG. 5: E_b and M are shown as a function of χ for 6×6 and 3×3 unit cells. Our results show that they agree well, suggesting that the 3×3 unit cell is large enough for TAHM.

D. Many-Body Correlation

The motivation to study the many-body correlation in this model comes from two perspectives. On one hand, the existence of TMO indicates that in each triangle there is probably some three-body correlation that is essentially different from the two-body correlation. Actually, this is one reason why we use PESS ansatz to study this model. On the other hand, from the view of quantum information, for mixed many-body states, generally the total correlation leaks more information than the part peculiar to quantum states only, i.e., entanglement, which has no classical counterpart [49]. What's more, though PESS is believed to be able to capture the many-body correlation better, there has no direct numerical evidence yet to demonstrate the existence of such correlation in the obtained wavefunction. Therefore, the frustrated TAHM offers such an opportunity to study the many-body correlation, especially the three-body correlation in a triangle.

To be specific, we envisage that the three spins $\{\sigma_a \sigma_b \sigma_c\}$ in a triangle comprise a mixed quantum state, which can be characterized by the reduced-density matrix $\rho^{(3)}$ defined below

$$\rho_{II'}^{(3)} = \sum_J |\Psi_{IJ}\rangle \langle \Psi_{I'J}| \quad (7)$$

where I and J denote the composite physical indices corresponding to $\{\sigma_a \sigma_b \sigma_c\}$ and the rest spins in the ground state, respectively. Similarly we can define $\rho^{(1)}$ for one spin and $\rho^{(2)}$ for a pair of spins sharing one bond.

Once the three kinds of mixed states are defined, we can calculate the von Neumann entropies, $S = -\text{Tr} \rho \ln \rho$, for these states. For simplicity, we use S_i, S_{ij}, S_{ijk} to denote the entropies corresponding to spin σ_i , spin pair $\sigma_i \sigma_j$ and spin simplex $\sigma_i \sigma_j \sigma_k$, respectively, with $i, j, k = a, b, c$. Then we measure the correlations in this small triangle through the following quantities defined below

$$\begin{aligned} I_a &= S_a \\ I_{ab} &= S_a + S_b - S_{ab} \\ I^{(3)} &= S_a + S_b + S_c - S_{abc} \end{aligned} \quad (8)$$

where I_{ab} and $I^{(3)}$ are the two-body and three-body mutual information which are used to measure the total correlation for a general quantum system [49], respectively. Other terms can be obtained similarly. Moreover, the true tripartite correlation $I_{tr}^{(3)}$, which is more relevant in this context, can be identified from $I^{(3)}$ by excluding the pair correlation contributions, i.e.,

$$I_{tr}^{(3)} = I^{(3)} - I_{ab} - I_{bc} - I_{ca} \quad (9)$$

The obtained results are shown in Fig. 6. We can see clearly that in this frustrated system, as D becomes larger, pair correlation becomes weaker, while simplex correlation becomes stronger. More importantly, it shows that as D increases, the true tripartite correlation $I_{tr}^{(3)}$ becomes more and more significant, which coincides with

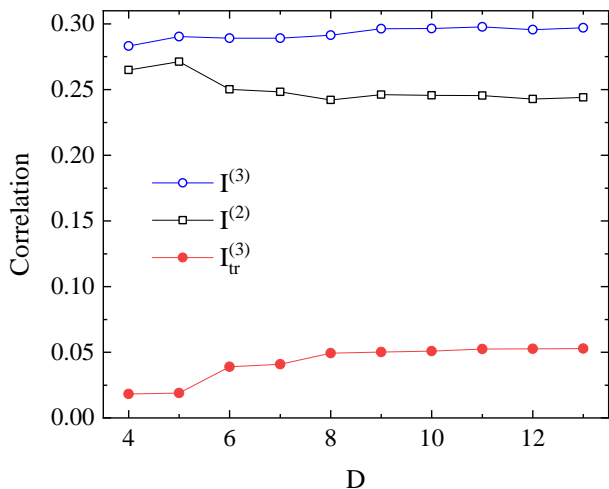


FIG. 6: Correlation measured by mutual information in one triangle of the ground-state wavefunction. Here, $I^{(2)}$ denotes the total pair correlation, namely $I^{(2)} = I_{ab} + I_{bc} + I_{ca}$. See Eq. (8) and (9).

the fact that the TMO can be argued to have imposed a global constrain on the three spins simultaneously, not just a local constrain on each pair in the triangle. This makes us more confident that the ground state should be of TMO, and that the PESS wavefunction can indeed grasp well the many-body correlation in this model.

IV. SUMMARY

In summary, using tensor-network algorithms with PESS-type trial wave function, we have studied the spin-1/2 antiferromagnetic Heisenberg model on the

triangular lattice. This wavefunction was optimized by the simple update imaginary-time evolution method, and the expectation values were estimated by the multi-sublattice CTMRG algorithm. By comparing the ground-state energy to that in other works, we confirmed that the wavefunction converges to the ground state and it is a TMO state. In particular, the magnetization is $M_0 = 0.161(5)$, which is smaller than that reported in previous calculations like GFMC, DMRG. Although frustration and quantum fluctuation do introduce some unusual properties into the model, such as roton-like excitations [21], its ground state remains magnetically ordered. This result is consistent with the correlation analysis, which shows that as D increases, the two-body correlation becomes weaker gradually, while the three-body correlation becomes increasingly significant. In viewing of the experience that TNS method, especially when simple update strategy is used, may tend to overestimate the magnetization of frustrated systems a little bit for a finite D , we believe that our work provides new benchmark results for this model.

V. ACKNOWLEDGEMENT

J. Z. is supported by the National Natural Science Foundation of China (Grant No. 11874188), H. L. is supported by the National Natural Science Foundation of China (Grant No. 11674139, 11834005), Z. Y. Xie is supported by the National R&D Program of China (Grants No. 2016YFA0300503 and No. 2017YFA0302900), the National Natural Science Foundation of China (Grants No. 11774420), and the Research Funds of Renmin University of China (Grants No. 20XNLG19). Qian Li and Hong Li contributed equally to this work.

-
- [1] P. W. Anderson, Mater. Res. Bull. **8**, 153 (1973)
 - [2] P. W. Anderson, Science **235**, 4793 (1987)
 - [3] F. Mila, Eur. J. Phys. **21**, 499 (2000)
 - [4] Y. Zhou, K. Kanoda, and T. K. Ng, Rev. Mod. Phys. **89**, 025003 (2017)
 - [5] L. Savary and L. Balents, Rep. Prog. Phys. **80**, 016502 (2017)
 - [6] P. A. Lee, Science **321**, 1306 (2008)
 - [7] L. Balents, Nature **464**, 199 (2010)
 - [8] D. A. Huse and V. Elser, Phys. Rev. Lett. **60**, 2531 (1988)
 - [9] D. Yoshioka and J. Miyazaki, J. Phys. Soc. Jpn. **60**, 614 (1991)
 - [10] L. O. Manuel, A. E. Trumper, and H. A. Ceccatto, Phys. Rev. B **57**, 8348 (1998)
 - [11] H. Nishimori and H. Nakanishi, J. Phys. Soc. Jpn. **57**, 626 (1988)
 - [12] B. Bernu, P. Lecheminant, C. Lhuillier, and L. Pierre, Phys. Rev. B **50**, 10048 (1994)
 - [13] J. Richter, J. Schulenburg, A. Honecker, and D. Schmalfuß, Phys. Rev. B **70**, 174454 (2004)
 - [14] N. Suzuki, F. Matsubara, S. Fujiki, and T. Shirakura, Phys. Rev. B **90**, 184414 (2014)
 - [15] L. Capriotti, A. E. Trumper, and S. Sorella, Phys. Rev. Lett. **82**, 3899 (1999)
 - [16] S. R. White and A. L. Chernyshev, Phys. Rev. Lett. **99**, 127004 (2007)
 - [17] S. Yunoki and S. Sorella, Phys. Rev. B **74**, 014408 (2006)
 - [18] S. A. Kulagin, N. Prokofev, O. A. Starykh, B. Svistunov, and C. N. Varney, Phys. Rev. Lett. **110**, 070601 (2013)
 - [19] C. Weber, A. Läuchli, F. Mila, and T. Giamarchi, Phys. Rev. B **73**, 014519 (2006)
 - [20] T. Xiang, J. Lou, and Z. Su, Phys. Rev. B **64**, 104414 (2001)
 - [21] W. Zheng, J. O. Fjærestad, R. R. P. Singh, R. H. McKenzie, and R. Coldea, Phys. Rev. B **74**, 224420 (2006)
 - [22] D. Heidarian, S. Sorella, and F. Becca, Phys. Rev. B **80**, 012404 (2009)
 - [23] A. L. Chernyshev and M. E. Zhitomirsky, Phys. Rev. B **79**, 144416 (2009); Erratum Phys. Rev. B **91**, 219905 (2015)

- [24] D. J. J. Farnell, O. Götze, J. Richter, and R. F. Bishop, and P. H. Y. Li, Phys. Rev. B **89**, 184407 (2014)
- [25] R. Kaneko, S. Morita, and M. Imada, J. Phys. Soc. Jpn. **83**, 093707 (2014)
- [26] E. A. Ghioldi, A. Mezio, L. O. Manuel, R. R. P. Singh, J. Oitmaa, and A. E. Trumper, Phys. Rev. B **91**, 134423 (2015)
- [27] P. H. Y. Li, R. F. Bishop, and C. E. Campbell, Phys. Rev. B **91**, 014426 (2015)
- [28] O. Götze, J. Richter, R. Zinke, and D. J. J. Farnell, J. Magn. Magn. Mater. **397**, 333 (2016)
- [29] E. A. Ghioldi, M. G. Gonzalez, Shang-Shun Zhang, Yoshitomo Kamiya, L. O. Manuel, A. E. Trumper, and C. D. Batista, Phys. Rev. B **98**, 184403 (2018)
- [30] H. D. Zhou, E. S. Choi, G. Li, L. Balicas, C. R. Wiebe, Y. Qiu, J. R. D. Copley, and J. S. Gardner, Phys. Rev. Lett. **106**, 147204 (2011)
- [31] Y. Li and Q. Zhang, J. Phys.: Condens. Matter **25**, 026003 (2013)
- [32] H. Niggemann and J. Zittartz, Z. Phys. B: Condens. Matter **101**, 289 (1996); H. Niggemann, A. Klumper, and J. Zittartz, *ibid.* **104**, 103 (1997)
- [33] T. Nishino, Y. Hieida, K. Okunishi, N. Maeshima, Y. Akutsu, and A. Gendiar, Prog. Theor. Phys. **105**, 409 (2001)
- [34] F. Verstraete and J. I. Cirac, arXiv:0407066 (2004)
- [35] H. C. Jiang, R. R. P. Singh, and L. Balents, Phys. Rev. Lett. **111**, 107205 (2013)
- [36] P. Corboz, T. M. Rice, and M. Troyer, Phys. Rev. Lett. **113**, 046402 (2014)
- [37] H. J. Liao, Z. Y. Xie, J. Chen, Z. Y. Liu, H. D. Xie, R. Z. Huang, B. Normand, and T. Xiang, Phys. Rev. Lett. **118**, 137202 (2017)
- [38] Z. Y. Xie, J. Chen, M. P. Qin, J. W. Zhu, L. P. Yang, and T. Xiang, Phys. Rev. B **86**, 045139 (2012)
- [39] C. Wang, S. M. Qin, and H. J. Zhou, Phys. Rev. B **90**, 174201 (2014)
- [40] M. Friesdorf, A. H. Werner, W. Brown, V. B. Scholz, and J. Eisert, Phys. Rev. Lett. **114**, 170505 (2015)
- [41] F. Verstraete and J. I. Cirac, Phys. Rev. Lett. **104**, 190405 (2010)
- [42] Y. Z. Liu, Y. Meurice, M. P. Qin, J. Unmuth-Yockey, T. Xiang, Z. Y. Xie, J. F. Yu, and H. Y. Zou, Phys. Rev. D **88**, 056005 (2013)
- [43] A. Tilloy and J. I. Cirac, Phys. Rev. X **9**, 021040 (2019)
- [44] Z. Y. Han, J. Wang, H. Fan, L. Wang, and P. Zhang, Phys. Rev. X **8**, 031012 (2018)
- [45] Z. F. Gao, S. Cheng, R. Q. He, Z. Y. Xie, H. H. Zhao, Z. Y. Lu, and T. Xiang, Phys. Rev. Research **2**, 023300 (2020)
- [46] Z. Y. Xie, J. Chen, J. F. Yu, X. Kong, B. Normand, and T. Xiang, Phys. Rev. X **4**, 011025 (2014).
- [47] T. Nishino and K. Okunishi, J. Phys. Soc. Jpn. **65**, 891 (1996)
- [48] R. Orús and G. Vidal, Phys. Rev. B **80**, 094403 (2009)
- [49] B. Zeng, X. Chen, D. L. Zhou, and X. G. Wen, *Quantum information meets quantum matter*, Springer (2019)
- [50] G. Vidal, Phys. Rev. Lett. **98**, 070201 (2007)
- [51] H. C. Jiang, Z. Y. Weng, and T. Xiang, Phys. Rev. Lett. **101**, 090603 (2008)
- [52] M. Lubasch, J. I. Cirac, and M. C. Banuls, Phys. Rev. B **90**, 064425 (2014)
- [53] Z. Y. Xie, H. J. Liao, R. Z. Huang, H. D. Xie, J. Chen, Z. Y. Liu, and T. Xiang, Phys. Rev. B **96**, 045128 (2017)